Journal of Magnetism and Magnetic Materials 565 (2023) 170275

Contents lists available at ScienceDirect

Journal of Magnetism and Magnetic Materials

journal homepage: www.elsevier.com/locate/jmmm

Preparation and thermogenic performance of monodisperse ferromagnetic Fe/SiO_2 nanoparticles for magnetic hyperthermia and thermal ablation*

Sun Qian-Jin[a,c], Dong Ming-Hong[a,c], Cai Hai-Chen[a,c], Zhang Xin-Yao[a,b], Lu Xue-Gang[d,*]

[a] Luoyang Ship Material Research Institute, Luoyang 471023, China
[b] Henan Key Laboratory of Technology and Application of Structural Materials for Ships and Marine Equipments, Luoyang 471023, China
[c] National New Material Production and Application Demonstration Platform (Advanced Marine Engineering and High-tech Ship Materials), Luoyang 471023, China
[d] MOE Key Laboratory for Non-Equilibrium Synthesis and Modulation of Condensed Matter, School of Physics, Xi'an Jiaotong University, Xi'an 710049, China

ARTICLE INFO

Keywords:
Fe/SiO_2 nanoparticles
Ferromagnetic property
Monodisperse
Magnetic hyperthermia
Thermal ablation

ABSTRACT

Ferromagnetic nanoparticles have great potential to be used in the field of magnetic hyperthermia and thermal ablation due to its high saturation magnetization (M_s) and high heating efficiency. In this paper, monodisperse spherical α-Fe_2O_3 nanoparticles were prepared by hydrothermal method using $FeCl_3$, $NaHCO_3$ and Na_2SO_4 as reactants. Then monodisperse Fe/SiO_2 nanoparticles with core/shell structure were obtained by coating SiO_2 on the surface of α-Fe_2O_3 nanoparticles and reducing at 500℃ in hydrogen atmosphere. The diameter of Fe core is about 230 nm and the thickness of SiO_2 coating is about 75 nm. Magnetic measurements show that Fe/SiO_2 nanoparticles exhibit typical ferromagnetic properties with M_s about 132.5 emu/g at 25 ℃. As-obtained Fe/SiO_2 nanoparticles have higher heating efficiency than superparamagnetic ferrite nanoparticles. The high heating ability of the Fe/SiO_2 nanoparticles is estimated to be related to the hysteresis loss and Brownian relaxation mechanism during alternating magnetization. The results show that Fe/SiO_2 nanoparticles are promising for the applications of magnetic hyperthermia and thermal ablation.

1. Introduction

In recent years, magnetic nanoparticles have attracted great attention due to their huge potential applications in magnetic targeted drug release, magnetic resonance imaging, and local thermotherapy [1–3]. The application of ferromagnetic nanoparticles in magnetic hyperthermia and thermal ablation treatment of tumors is one of the most interesting research topics [4–7]. A major advantage of magnetic hyperthermia and thermal ablation therapy is that it can locally generate heat and selectively kills malignant tumor cells [8]. Therefore, the drug dose required is small and the side effects on the human body are low.

So far, quite a lot of research on the possibility of magnetic nanoparticles used in magneto-hyperthermia has been carried on. But most of the researches are focused on superparamagnetic iron oxide nanoparticles [9–13]. With the lower energy conversion rate, it is necessary to increase the injection dose of such ultra-small iron oxide nanoparticles to achieve the expected magnetic hyperthermia effect [14] in most practical clinical applications. To further improve the efficiency of heat generation, materials with high magnetic moments have attracted more and more attention from researchers [15,16]. Theoretically, the heat generation mechanism of superparamagnetic iron oxide nanoparticles usually includes Néel relaxation and Brownian relaxation [17]. Néel relaxation is generated by the rotation of the magnetic moment around the crystal axis inside the nanocrystal. Under the alternating magnetic field, the rotating motion of the magnetic moment converts the magnetic field energy into heat energy. Energy generated by Brownian relaxation is caused by the rotation and friction of particles in the solution under an alternating magnetic field. However, for ferromagnetic nanoparticles, besides Néel relaxation and Brownian relaxation, hysteresis loss is another important source of heat generation [18]. It is well known that ferromagnetic materials have hysteresis characteristics, and the area of the hysteresis loop represents the energy loss per unit volume [19]. The hysteresis loss increases with the increase of magnetic induction intensity and anisotropy barrier. The high saturation magnetization and large magnetocrystalline anisotropic barrier of ferromagnetic nanoparticles help them to become efficient heat sources in magnetic hyperthermia therapy, especially thermal ablation therapy [20]. Ferromagnetic metals, including Fe, Co, Ni and FeCo, FeNi alloy nanoparticles, have high magnetic moments, but the poor chemical stability and biocompatibility limit their applications in the biomedical field.

* Corresponding author.
E-mail address: xglu@mail.xjtu.edu.cn (X.-G. Lu).

https://doi.org/10.1016/j.jmmm.2022.170275
Received 15 January 2022; Received in revised form 10 November 2022; Accepted 5 December 2022
Available online 8 December 2022

Coating SiO_2 on the surface of ferromagnetic metal nanoparticles can not only improve the chemical stability and biocompatibility, but also provide polar surface for the attachment of drug molecules and surfactants [21].

Here, we present a facile chemical method to synthesize monodisperse ferromagnetic Fe/SiO_2 composite nanoparticles, and found that the nanoparticles have strong heating ability under alternating magnetic field. As-prepared ferromagnetic nanoparticles are expected to have potential applications in the fields of magnetic hyperthermia, thermal ablation, etc.

2. Experiments

2.1. Materials

Ferric chloride hexhydrate ($FeCl_3{\cdot}6H_2O$), sodium bicarbonate ($NaHCO_3$), sodium sulfate (Na_2SO_4), ethyl orthosilicate (TEOS, 98 %) and ammonia (28 %) were purchased from Shanghai Chemical Reagent Company. All the chemicals are analytical grade and directly used as received without any further purification. The water used in the experiment was de-ionized water.

2.2. Synthesis of monodisperse spherical α-Fe_2O_3 nanoparticles

20 mL $FeCl_3{\cdot}6H_2O$ (0.02 mol/L), 48 mL $NaHCO_3$ (1 mmol/L) and 12 mL Na_2SO_4 (1 mmol/L) were mixed together, magnetically stirred for 10 min, and transferred into a stainless steel autoclave with a capacity of 100 mL, and heated for reaction at 220℃ for 10 h. After the reaction, the autoclave was cooled to room temperature. The products were centrifugally separated from the solution, washing with de-ionized water and ethanol repeatedly, drying at 60℃, and collecting for later use.

2.3. Preparation of monodisperse Fe/SiO_2 nanoparticles

60 mg α-Fe_2O_3 powder was ultrasonically dispersed in de-ionized water of 50 mL to obtain a brick-red suspension. 0.5 mL TEOS and 3 mL absolute ethanol were added into the suspension under stirring to form a well-mixed solution. Subsequently, 5 mL ammonia was added drop wise. The reaction lasted for 30 min in an ice water bath. Finally, the products were magnetically separated from the solution, washing with de-ionized water and ethanol repeatedly, drying at 60℃, to obtain α-Fe_2O_3/SiO_2 composite nanoparticles.

The product above is placed in a quartz tube, reduced in a hydrogen atmosphere at 500 °C for 30 min to obtain the final Fe/SiO_2 composite nanoparticles.

2.4. Characterization

The d8-advance 3.0 X-ray diffraction (XRD) produced by Bruker in Germany was used for phase analysis of the samples. The field emission scanning electron microscope (FE-SEM, JSM-7000F) and high resolution transmission electron microscope (HRTEM, JEOL-2100F) were used to analyze the morphology of the sample. The energy-dispersive X-ray spectroscopy (EDS) line scans were performed on Scios 2 Dual-Beam FIB SEM to analyze the chemical composition of the particles. Quantum Design's SQUID comprehensive physical property analyzer was used to test the magnetic properties of the product.

To evaluate the heat generation efficiency of Fe/SiO_2 composite nanoparticles, the Fe/SiO_2 nanoparticles were ultrasonically dispersed in physiological saline of 5 mL to form a colloidal solution with a concentration of 10 mg/mL. The colloidal solution was placed in a transparent biological glass test tube, and the instantaneous temperature of the solution was measured with a kerosene thermometer under an alternating magnetic field to evaluate the heating performance of the sample. The alternating magnetic field was generated by an alternating magnetic field generator, the alternating excitation coil is composed of 5 turns of copper pipe, and the coil temperature is controlled at 23℃ by circulating cooling water.

3. Results and discussion

The SEM and TEM images of the synthesized α-Fe_2O_3 and Fe/SiO_2 composite nanoparticles are shown in Fig. 1. It can be seen from Fig. 1a that the α-Fe_2O_3 nanoparticles produced by the hydrothermal reaction are typical monodisperse spherical nanoparticles with particle size about 240 nm. After being coated with SiO_2 and reduced at 500℃ in hydrogen atmosphere, the products still maintain monodisperse spherical morphology, as shown in Fig. 1b and1c. Due to the presence of the SiO_2 coating layer, the overall particle size increases to about 380 nm. It can be further seen from the enlarged TEM image in Fig. 1d that the coated and reduced particles have a typical core/shell structure. The darker area in the center of the particle represents Fe core with a diameter of about 230 nm formed after reduction. The lighter colored peripheral portion represents the SiO_2 coating layer, with a thickness of about 75 nm. It can also be seen from Fig. 1d that after the hydrogen reduction process at 500 °C, the sphericity of the Fe/SiO_2 composite particles maintains well, and there is no obvious agglomeration and adhesion between the particles. In order to confirm the chemical composition of the core and shell of the particles, EDS analysis was performed on the as-synthesized Fe/SiO_2 nanoparticles. The result is shown in Figure S1. The distribution profiles of Si and Fe elements further prove that the synthesized Fe/SiO_2 nanoparticles have a typical core–shell structure. The product reduced can be readily re-dispersed in physiological saline and other solvents with the assistance of ultrasonic vibration. The uniform colloidal solution formed after dispersion shows high response ability to external magnetic field. When the magnet approaches the solution, the magnetic particles quickly gather toward the magnet. When the magnet is moved away, the magnetic particles are rapidly re-dispersed in the medium.

Fig. 2 shows the XRD results of the samples before and after hydrogen reduction. As can be seen from Fig. 2 that all the diffraction peaks of the samples synthesized by the hydrothermal method correspond to the XRD characteristic peaks of the rhombohedra α-Fe_2O_3 phase (hematite) provided in the standard PDF card (JCPDS file 89–0597). No impurity peaks of β-FeOOH, Fe_3O_4 or γ-Fe_2O_3 appear, indicating that the sample is composed of high purity α-Fe_2O_3 phase. The sharp diffraction peaks indicate that the sample obtained is well crystallized. The XRD diffraction peaks of the reduced sample agree with the characteristic peaks of the cubic α-Fe phase provided in the standard PDF card (JCPDS file 65–4899). The diffraction peaks at the diffraction angle of $2\theta = 44.6^\circ$ and 65.0° correspond to the (1 1 0) and (2 0 0) crystal planes of α-Fe phase respectively. No other impurity peaks can be observed, indicating that α-Fe_2O_3 is completely reduced into pure Fe metal after reduction in hydrogen atmosphere at 500℃. The flat amorphous diffraction peak near $2\theta = 20^\circ$ in the XRD diffraction spectrum implies that the SiO_2 in the reduced product is in amorphous form. In order to confirm the chemical composition of the core and shell of the particles, EDS analysis was performed on the as-synthesized Fe/SiO_2 nanoparticles. The result is shown in Figure S1. The distribution profiles of Si and Fe elements further prove that the synthesized Fe/SiO_2 nanoparticles have a typical core–shell structure. The SiO_2 coating layer not only helps to improve the hydrophilicity of the particles, but also prevents corrosion and oxidation caused by the interaction between internal Fe nanoparticles and surrounding medium. Further experiments show that the XRD diffraction spectrum of Fe/SiO_2 sample stored in air and normal saline for 3 months has no significant change compared with its initial state, indicating that the product has high chemical stability, as shown in Figure S2.

It is well known that α-Fe_2O_3 crystal belongs to the hexagonal crystal system. Due to the inconsistent growth rate of different crystal planes in the hydrothermal reaction process, rod-like, needle-like, sheet-like and other polyhedral shapes are easy to appear in the product. The formation

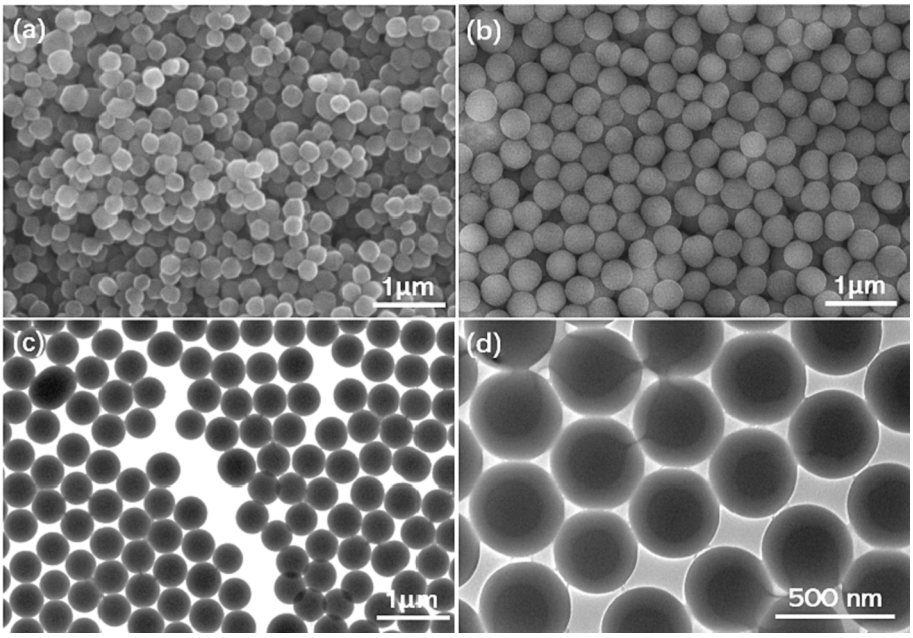

Fig. 1. SEM image of α-Fe_2O_3 nanoparticles synthesized by hydrothermal method (a), SEM (b) and TEM (c, d) images of Fe/SiO_2 composite particles obtained by reduction.

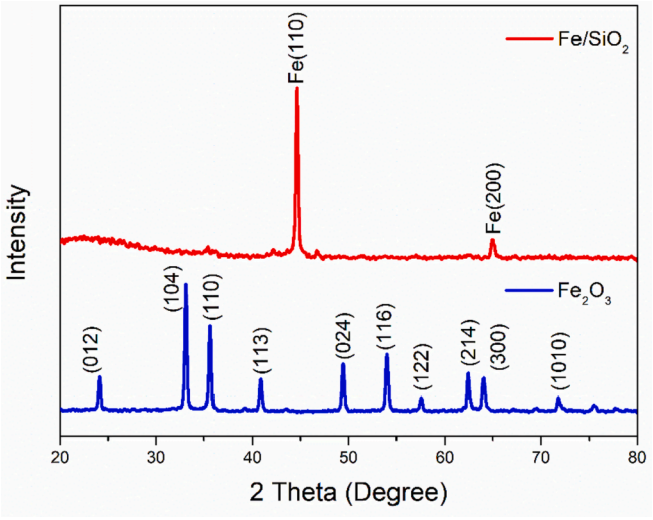

Fig. 2. XRD patterns of α-Fe_2O_3 nanoparticles synthesized by hydrothermal method and Fe/SiO_2 composite particles after hydrogen reduction.

of α-Fe_2O_3 nanoparticles with different shapes is mainly related to the selective adsorption of the additives of $NaHCO_3$ and Na_2SO_4 on different crystal planes, which causes the crystals to grow along a specific direction. Since $FeCl_3$ generates H^+ during the hydrolysis reaction to form α-Fe_2O_3, the local portion of the solution appears to be acidic (pH less than 7.0). Under acidic environment and high temperature of 220 °C, the initially formed particles may locally dissolve with the following reaction:

$$Fe_2O_3 + 6H^+ \rightarrow 2Fe^{3+} + 3H_2O \quad (1)$$

Therefore, during the formation of α-Fe_2O_3 particles, the crystallization process and the dissolution process proceed simultaneously.

The sulfate ions play a major role in the dissolution of α-Fe_2O_3 particles. When the concentration of sulfate ions is high, the resulting particles tend to be flake-shape. Sulfate ions and ferric ions will react according to the following equation:

$$Fe^{3+} + xSO_4^{2-} \rightarrow [Fe(SO_4)_x]^{3-2x} \quad (2)$$

The bicarbonate ion can be adsorbed on the specific crystal planes of the α-Fe_2O_3 particles, which restrict the growth of the corresponding crystal planes. Thus, the synergistic effect of bicarbonate and sulfate can determine the final morphology of α-Fe_2O_3 particles. During the experiment, it is found that when the molar ratio of HCO_3^- and SO_4^{2-} is relatively small (1:4), the morphology of α-Fe_2O_3 nanoparticles obtained are in the form of flakes. As the ratio of the two ions increases to 4:1, the morphology of the particles is nearly spherical shape. The morphology of α-Fe_2O_3 nanoparticles will affect the morphology of the particles after the subsequent SiO_2 coating, and it also affect the morphology of the final reduction product. Therefore, controlling the morphology of α-Fe_2O_3 nanoparticles and obtaining spherical nanoparticles is one of the important goals pursued in this experiment.

To further investigate the magnetic properties of the product, the room temperature magnetism of the sample before and after reduction was tested with SQUID, and the results are shown in Fig. 3. It can be seen from Fig. 3(a) that the α-Fe_2O_3 nanoparticles synthesized are of weak ferromagnetism, with coercivity of about 260Oe and remanence of about 2.0 emu/g. As can be seen from Fig. 3(b) that the Fe/SiO_2 composite particles obtained by reduction exhibit typical ferromagnetism. The saturation magnetization of the Fe/SiO_2 composite particles is as high as 132.5 emu/g and the coercivity is approximately 180Oe, which indicates that α-Fe_2O_3 nanoparticles are converted into Fe after the reduction reaction under 500°C. Compared with the saturation magnetization of pure bulk Fe (M_s≈220 emu/g), the saturation magnetization of Fe/SiO_2 composite particles is reduced because of the presence of non-magnetic SiO_2 in the sample which dilutes the magnetic properties of Fe. Compared with Fe_3O_4 nanoparticles, Fe/SiO_2 nanoparticles have higher magnetization, which gives them significant advantages in magnetic response, magnetic separation, and magnetic heating.

To evaluate the heating ability of the synthesized Fe/SiO_2 nanoparticles under alternating magnetic field, we dispersed the Fe/SiO_2 nanoparticles in standard physiological saline to form a suspension with a concentration of 10 mg/mL, and measured the temperature change with time in alternating magnetic field. Fig. 4 shows the temperature–time curves of Fe/SiO_2 nanoparticles in physiological saline under alternating magnetic fields with different strengths. It can be seen from

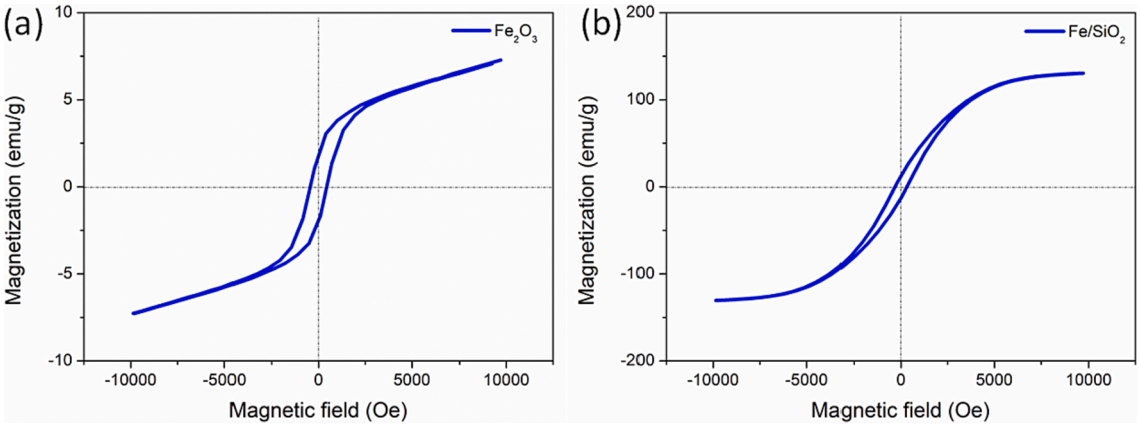

Fig. 3. Room temperature hysteresis loops of α-Fe_2O_3 (a) and Fe/SiO_2 samples (b).

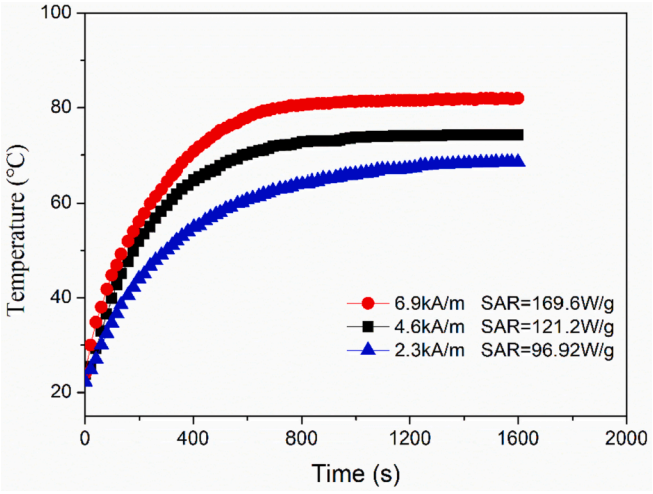

Fig. 4. Time-dependent heating curves acquired at 55 kHz and various magnetic field strength.

Fig. 4 that under the alternating magnetic field of 55 kHz (the magnetic field strength is 2.3kAm^{-1}, 4.6kAm^{-1}, 6.9kAm^{-1} respectively), the temperature of the sample with a concentration of 10 mg/mL can reach saturation after 20 min, and the saturation temperatures are 67.2℃, 74.5℃ and 81.5℃ respectively. Obviously, when the frequency of the alternating magnetic field remains the same, the greater the magnetic field strength, the shorter the time required to reach the saturation temperature. In addition, the magnetic heating ability of Fe/SiO_2 nanoparticles can be quantified through the specific absorption rate (SAR) as the following equation[22]:

$$\mathrm{SAR} = \frac{\sum_i C_i m_i}{m_{sample}} \frac{\Delta T}{\Delta t} \tag{3}$$

Where C_i represents the heat capacity of each component (C_{water} = 4.2 J/(g·K), C_{SiO_2}=1.0 J/(g·K), C_{Fe}= 0.46 J/(g·K)), m_i represents the mass of the each component, $\Delta T/\Delta t$ represents the maximum slope on the temperature–time curve. It can be seen that the SAR value is related to the field strength of the alternating magnetic field. As the field strength increases from 2.3kAm^{-1} to 4.6kAm^{-1} and 6.9kAm^{-1}, the SAR value rises from 96.92 W/g to 121.2 W/g and 169.6 W/g respectively. In order to evaluate the heat generating ability of the synthesized particles, we compared the results with the Fe_3O_4/SiO_2 composite particles we reported previously[23]. For the Fe_3O_4/SiO_2 sample, the diameter of Fe_3O_4 core is about 260 nm, and there is almost no coercivity and remanence. Under almost the same measuring conditions (4.6kA/m, 55 kHz, and10mg/mL), the heating efficiency of Fe/SiO_2 is significantly higher than that of Fe_3O_4/SiO_2 composite particles. In the same heating time, the temperature of the former is significantly higher than that of the latter. The results above imply that the as-prepared Fe/SiO_2 nanoparticles have the potential to be used in magnetic hyperthermia and thermal ablation therapy.

At present, the mechanism of magnetic hyperthermia is not fully understood, despite multiple previous theoretical and experimental studies. Under AC magnetic field, it is generally believed that there are several different heat generation mechanisms, including eddy current loss, hysteresis loss, Brownian relaxation and Néel relaxation. Among them, eddy current heating for small magnetic particles is negligible compared to other magnetic losses[24]. For the Fe/SiO_2 composite particles synthesized in this paper, although XRD has proved that the core is α-Fe and there are no Fe silicate phases formed, the eddy current loss is negligible due to the small particle size. Néel relaxation depends on the magnetic characteristics of the nanoparticles and is caused by the fluctuation of the magnetic moment over anisotropic energy barrier. Néel relaxation usually occurs in superparamagnetic particles (less than 30 nm for iron oxide). In this case, an external AC magnetic field supplies energy and assists magnetic moments to rotate in overcoming the energy barrier $E \sim KV$, where K is the anisotropy constant and V is the volume of the magnetic core. This energy is dissipated when the particle moment relaxes to its equilibrium orientation (Néel relaxation). For the larger size ferromagnetic particles, the fluctuation of the magnetic moment over anisotropic energy barrier is not easy to occur, so it is unlikely to generate heat through Néel relaxation. Brownian relaxation is caused by the rotation of the particle as a whole. In the Brownian relaxation mode, the interaction between a thermal force and viscous drag in the suspending medium will influence the particle movement significantly. The whole particle moves towards the external field with the moment locked along the crystal axis instead. This phenomenon serves to account for the mechanical friction component in a given suspending medium. Brownian relaxation can occur not only in ultra-small superparamagnetic particles, but also in larger magnetic particles with weak dipolar interaction. Previous studies have shown that for large magnetic particles in the ferromagnetic regime, besides the Brownian relaxation loss, the hysteresis loss plays significant role in the heat generation[25–27]. In this experiment, the SiO_2 coating with a thickness of 150 nm would weaken the dipolar-interaction between Fe particles, so the contribution of Brownian relaxation loss to heat generation cannot be excluded. In addition, as mentioned above, our samples consist of multi-domain Fe core with a mean diameter of 230 nm (The single domain critical size of Fe is about 20 nm). For such large nanoparticles, hysteresis plays the significant role for heating[28], since the domain walls exist and their pinning creates power losses. For large particles (>100 nm), which exhibit ferromagnetic behavior, hysteresis losses per cycle depend on the field according to a third-order power

law, usually indicated as the Rayleigh law[12]. On the other hand, the dissipated magnetic energy is proportional to H^2 for superparamagnetic nanoparticles[27]. In this experiment, although the intensity of the applied alternating magnetic field did not exceed the coercive force of the particles (≈180Oe), and the area of hysteresis loop obtained is quite small, the heating efficiency of Fe/SiO_2 is still significantly higher than that of large size, superparamagnetic Fe_3O_4/SiO_2 composite particles, indicating that the power loss of hysteresis should not be ignored. With the increase of magnetic field intensity, the area of hysteresis loop will increase, and thus the heat generation efficiency will also increase, as shown in Fig. 4.

The analysis results above reveal that the as-prepared monodisperse Fe/SiO_2 nanoparticles have high heating efficiency, and are expected to be used in magneto-hyperthermia and thermal ablation treatment of tumors.

4. Conclusions

In this paper, monodisperse spherical α-Fe_2O_3 nanoparticles were prepared by hydrothermal method with $FeCl_3$, $NaHCO_3$ and Na_2SO_4 as raw materials. On this basis, α-Fe_2O_3 nanoparticles were coated with SiO_2 and further reduced in hydrogen atmosphere at 500℃ to obtain monodisperse Fe/SiO_2 core/shell structured nanoparticles. The existence of the SiO_2 coating layer greatly improves the chemical stability of Fe nanoparticles. The results of magnetic measurements show that the as-prepared monodisperse Fe/SiO_2 nanoparticles are of typical ferromagnetism, with a saturation magnetization of 132.5 emu/g at 25 °C and a coercivity of about 260Oe. Under the alternating magnetic field of 55 kHz (the magnetic field strength is 2.3kAm^{-1}, 4.6kAm^{-1}, 6.9kAm^{-1}, respectively), the sample prepared by dispersing Fe/SiO_2 nanoparticles in physiological saline with a concentration of 10 mg/mL can reach the saturation temperature of 67.2℃, 74.5℃ and 81.5℃after 20 min, and the corresponding SAR values were 96.92 W/g, 121.2 W/g and 169.6 W/g, respectively. The high heat generation ability is estimated to be related to the hysteresis loss and Brownian relaxation during the magnetization process. The ferromagnetic Fe/SiO_2 nanoparticles have potential application prospects in magnetic hyperthermia and thermal ablation therapy.

Declaration of Competing Interest

The authors declare that they have no known competing financial interests or personal relationships that could have appeared to influence the work reported in this paper.

Data availability

Data will be made available on request.

Appendix A. Supplementary material

Supplementary data to this article can be found online at https://doi.org/10.1016/j.jmmm.2022.170275.

References

[1] A. Cervadoro, M. Cho, J. Key, C. Cooper, C. Stigliano, S. Aryal, A. Brazdeikis, J. F. Leary, P. Decuzzi, ACS Appl. Mater. Inter. 6 (2014) 12939.
[2] Y.V. Kolen'ko, M. Banobre-Lopez, C. Rodriguez-Abreu, E. Carbo-Argibay, A. Sailsman, Y. Pineiro-Redondo, M. Fatima Cerqueira, D.Y. Petrovykh, K. Kovnir, O.I. Lebedev, J. Rivas, J. Phys. Chem. C 118 (2014) 8691.
[3] P. Hugounenq, M. Levy, D. Alloyeau, L. Lartigue, E. Dubois, V. Cabuil, C. Ricolleau, S. Roux, C. Wilhelm, F. Gazeau, R. Bazzi, J. Phys. Chem. C 116 (2012) 15702.
[4] K. Simeonidis, C. Martinez-Boubeta, L. Balcells, C. Monty, G. Stavropoulos, M. Mitrakas, A. Matsakidou, G. Vourlias, M. Angelakeris, J. Appl. Phys. 114 (2013).
[5] K.N. Collier, N.J. Jones, K.J. Miller, Y.L. Qin, D.E. Laughlin, M.E. McHenry, J. Appl. Phys. 105 (2009).
[6] A. Chalkidou, K. Simeonidis, M. Angelakeris, T. Samaras, C. Martinez-Boubeta, L. Balcells, K. Papazisis, C. Dendrinou-Samara, O. Kalogirou, J. Magn. Magn. Mater. 323 (2011) 775.
[7] Y. Jing, H. Sohn, T. Kline, R.H. Victora, J.-P. Wang, J. Appl. Phys. 105 (2009).
[8] B. Mehdaoui, R.P. Tan, A. Meffre, J. Carrey, S. Lachaize, B. Chaudret, M. Respaud, Phys. Rev. B 87 (2013).
[9] P. Guardia, R. Di Corato, L. Lartigue, C. Wilhelm, A. Espinosa, M. Garcia-Hernandez, F. Gazeau, L. Manna, T. Pellegrino, Acs Nano 6 (2012) 3080.
[10] N.V. Jadhav, A.I. Prasad, A. Kumar, R. Mishra, S. Dhara, K.R. Babu, C.L. Prajapat, N.L. Misra, R.S. Ningthoujam, B.N. Pandey, R.K. Vatsa, ColloidSurface B 108 (2013) 158.
[11] A.P.R. Mary, T.N. Narayanan, V. Sunny, D. Sakthikumar, Y. Yoshida, P.A. Joy, M. R. Anantharaman, Nanoscale Res. Lett. 5 (2010) 1706.
[12] M. Elisa de Sousa, M.B. Fernandez van Raap, P.C. Rivas, P. Mendoza Zelis, P. Girardin, G.A. Pasquevich, J.L. Alessandrini, D. Muraca, F.H. Sanchez, J. Phys. Chem. C (2013) 117 5436.
[13] S. Laurent, S. Dutz, U.O. Haefeli, M. Mahmoudi, Adv. ColloidInterface 166 (2011) 8.
[14] K. Maier-Hauff, F. Ulrich, D. Nestler, H. Niehoff, P. Wust, B. Thiesen, H. Orawa, V. Budach, A. Jordan, J. Neuro-Oncol. 103 (2011) 317.
[15] Y.H. Xu, H. Bai, J.P. Wang, J. Magn. Magn. Mater. 311 (2007) 131.
[16] K.L. McNerny, Y. Kim, D.E. Laughlin, M.E. McHenry, J. Appl. Phys. 107 (2010).
[17] S. Mornet, S. Vasseur, F. Grasset, E. Duguet, J. Mater. Chem. 14 (2004) 2161.
[18] J. Carrey, B. Mehdaoui, M. Respaud, J. Appl. Phys. 109 (2011).
[19] E. Kita, T. Oda, T. Kayano, S. Sato, M. Minagawa, H. Yanagihara, M. Kishimoto, C. Mitsumata, S. Hashimoto, K. Yamada, N. Ohkohchi, J. Phys. DAppl. Phys. 43 (2010).
[20] X. Lu, J. Wu, G. Huo, Q. Sun, Y. Huang, Z. Han, G. Liang, Colloid Surfaces A414 (2012) 168.
[21] L. Zhu, Z. Ai, W. Ho, L. Zhang, Purif. Technol. 108 (2013 Sep) 159.
[22] G. Liu, M. Kawashita, Z. Li, T. Miyazaki, H. Kanetaka, J. Sol-Gel Sci. Techn. 75 (2015) 90.
[23] X. Lu, Q. Liu, L. Wang, W. Jiang, W. Zhang, X. Song, RSC Adv. 7 (2017) 32049.
[24] M.M. Goswami, C. Dey, A. Bandyopadhyay, D. Sarkar, M. Ahir, J. Magn. Magn. Mater. 417 (2016) 376.
[25] E.B. Stephen, Int. J. Hyperthermia 24 (2008) 451.
[26] Q. Zeng, I. Baker, J.A. Loudis, Y. Liao, P.J. Hoopes, J.B. Weaver, Appl. Phys. Lett. 90 (2007) 233112.
[27] P. Hiergeist, W. Andrä, N. Buske, R. Hergt, I. Hilger, U. Richter, W. Kaiser, J. Magn. Magn. Mater. 201 (1999) 420.
[28] K.D. Bakoglidis, K. Simeonidis, D. Sakellari, G. Stefanou, M. Angelakeris, IEEE T. Magn. 48 (2012) 1320.